RSC Advances

PAPER

View Article Online
View Journal | View Issue

Cite this: *RSC Adv.*, 2018, **8**, 14870

Effective solvent-free oxidation of cyclohexene to allylic products with oxygen by mesoporous etched halloysite nanotube supported Co^{2+}†

Cuiping Li,* Yue Zhao, Tianwen Zhu, Yan'ge Li, Jiajia Ruan and Guanghui Li

One dimensional mesoporous etched halloysite nanotube supported Co^{2+} is achieved by selective etching of Al_2O_3 from halloysite nanotube (HA) and immersing the etched HA (eHA) into the $Co(NO_3)_2 \cdot 6H_2O$ solution consecutively. By facilely tuning the etching time and the weight ratio of $Co(NO_3)_2 \cdot 6H_2O$ to eHA, the morphology, specific surface area and the supported Co^{2+} content of the mesoporous material can be tuned. The method for mesoporous material is scaled up and can be extended to other clay minerals. The mesoporous eHA supported Co^{2+} is used as catalyst for the selective catalytic oxidation of cyclohexene in solvent-free reaction system with O_2 as oxidant. The results shows the catalytic activity is dependent on etching time, weight ratio of $Co(NO_3)_2 \cdot 6H_2O$ to eHA, calcination treatment and reaction time/temperature. Among them, mesoporous eHA supported Co^{2+} prepared with 18 h etching time and 2 : 1 $Co(NO_3)_2 \cdot 6H_2O$/eHA weight ratio without calcination (HA/HCl-18 h/Co^{2+}-2 : 1) demonstrates the highest catalytic activity under 75 °C reaction temperature and 18 h reaction time (58.30% conversion and 94.03% selectivity to allylic products). Furthermore, HA/HCl-18 h/Co^{2+}-2 : 1 has exhibit superior cycling stability with 37.69% conversion and 92.73% selectivity to allylic products after three cycles.

Received 12th October 2017
Accepted 9th April 2018

DOI: 10.1039/c7ra11245a

rsc.li/rsc-advances

1 Introduction

Cyclohexene oxidation is an important reaction for the synthesis of oxygen-containing intermediates such as epoxy cyclohexane, 1,2-cyclohexanediol, adipic acid, 2-cyclohexen-1-one, 2-cyclohexen-1-ol and cyclohexene peroxide, which widely applies in medicine, pesticides, spices, surfactant and polymer area.[1] Among various oxidation products, allylic oxidation products (2-cyclohexen-1-one and 2-cyclohexen-1-ol) arouse particularly attention because of their multifarious application in pharmaceutical, chemical and material industries.[2–4] However, due to the presence of multiple oxidation sites-unsaturated C=C double bond and α-H atoms, cyclohexene oxidation usually accompanies poor selectivity to allylic product, which will result in complex oxidation products and difficulty in separation.[5] The commonly catalysts for the catalytic oxidation of cyclohexene to allylic product is supported metal based catalyst as they have the advantage of high stability, high catalytic activity and easy separation and recycling[6–15] when compared with the homogeneous catalyst system. For various supports for metal based catalyst, mesoporous materials with tunable pore size, large specific surface area and good stability are extensively investigated.[12–15] Through surface modification of the mesoporous material, and the active center coordination with the homogeneous catalyst, the mesoporous material supported catalyst is obtained and demonstrates good cyclohexene catalytic oxidation activity. For example, Khalili *et al.* support metal porphyrin (Mn(III)TClPPCl, Fe(III)TClPPCl and Co(III)TClPPCl) on MCM-48, and achieve 80% cyclohexene conversion and 95% selectivity to 2-cyclohexen-1-one with MCM-48 supported Fe(III)TClPPCl as catalyst and TBHP as oxidant in CH_3CN at 60 °C.[12] Rahiman *et al.* demonstrate MCM-41 supported metal porphyrins have various selectivity: the main oxidation product is epoxy cyclohexane when with MCM-41 supported manganoporphyrin as catalyst; whereas the main oxidation product is allylic products when with MCM-41 supported ferriporphyrin as catalyst.[13] Park *et al.* prepare mesoporous silica with porphyrin structure by microwave co-condensation, and Fe(III) as the central atom is introduced into porphyrin by ion exchange. The mesoporous silica supported ferriporphyrin exhibits 41.5% cyclohexene conversion and 68.9% selectivity to allylic product at 60 °C.[14] However, to form uniform and ordered pore channels, soft template agent and high temperature calcinations are usually involved in, which result in complicated, time-consuming and energy consumption preparation process.

On the other hand, halloysite nanotube is a type of natural occurring clay minerals with nanotubular structures and consists of two-layered aluminosilicate with a chemical composition of $Al_2Si_2O_5(OH)_4 \cdot nH_2O$).[16] Its structure and

School of Chemical Science and Technology, Key Laboratory of Medicinal Chemistry for Natural Resource, Ministry of Education, Yunnan University, Kunming 650091, China. E-mail: licp830@iccas.ac.cn; Fax: +86 871 6503 1567

† Electronic supplementary information (ESI) available: Data of HA, eHA and eHA@Co^{2+}; effect of reaction condition on cyclohexene oxidation and recycling stability study with HA/HCl-18 h/Co^{2+}-*R* as catalyst. See DOI: 10.1039/c7ra11245a

chemical composition is similar to that of kaolinite, dickite or nacrite except for the unit clay layers are separated by a monolayer of water molecules.[17] Compared to other supports, halloysite nanotube has the advantage of abundant reserves, high porosity and excellent chemical stability, which is usually utilized as an attractive support for catalyst.[18–27] In our previous studies,[24] it has been demonstrated that mesoporous SiO_2 and SiO_2/Al_2O_3 can been controlled synthesized in large scale by selective etching of the interior Al_2O_3 from hydrophobically modified halloysite nanotube or halloysite nanotubes by HCl. As the selective etching by HCl is the positive charged Al_2O_3, the surface of the etched halloysite nanotubes should be negative charged and can induce the adsorption of metal cation to achieve mesoporous etched halloysite nanotubes supported metal ions. Although mesoporous material supported metal cation has already been used in cyclohexene oxidation, mostly involves in supported metal compounds and complicated modification/treatment before supporting. And it is usually conducted with toxic, volatile solvent and expensive oxidant.[12–15] For all we know, the influence of etching time, weight ratio of $Co(NO_3)_2 \cdot 6H_2O$ to etched HA (eHA) in the fabrication on the cyclohexene oxidation activity of mesoporous eHA supported Co^{2+} (eHA@Co^{2+}), especially the environment-friendly cyclohexene oxidation process (solvent-free, O_2 as oxidant and only bubbling with O_2 a few minutes before oxidation reaction) and effective catalytic activity (58.30% conversion and 94.03% selectivity to allylic products) have rarely been reported.

In this study, the mesoporous eHA supported Co^{2+} (eHA@Co^{2+}) are prepared through HCl selective etching and *in situ* Co^{2+} adsorption, consecutively. By simply tuning the etching time and feeding amount of Co^{2+} in the preparation, mesoporous eHA@Co^{2+} with different BET specific surface area and Co^{2+} content can be achieved. The influence of catalyst (etching time, feeding amount of Co^{2+} and calcination in the preparation) and reaction condition (reaction time/temperature, solvent and oxidant) on the cyclohexene selective oxidation of mesoporous eHA@Co^{2+} are investigated in detail. In addition, the cycling stability of eHA@Co^{2+} is also investigated. In line with the results, a mechanism for cyclohexene oxidation is proposed.

2 Experimental

2.1 Materials

Halloysite nanotubes were purchased from Fenghui Minerals Trade Co., Ltd. Cobalt(II) nitrate hexahydrate ($Co(NO_3)_2 \cdot 6H_2O$) and cyclohexene (99%) were purchased from Shanghai Titan Scientific Co., Ltd. Hydrochloric acid (HCl), ethanol and trichloromethane ($CHCl_3$) were purchased from Chongqing Chuandong Chemical (Group) Co., Ltd. O_2 (99.99%) was purchased from Kunming Messer Gases Products Co., Ltd. All the chemical reagents were analytical grade and used directly.

2.2 Selective etching of halloysite nanotubes

In the preparation of mesoporous etched halloysite nanotube (eHA), the amounts of halloysite nanotubes and 36–38% HCl were constant and the etching degree and morphology of eHA were regulated by the etching time. A typical procedure to prepare mesoporous eHA was as follows:[24] HCl solution (36–38%, 350 mL) and halloysite nanotubes (6.25 g) were added into a 500 mL round flask. After dispersion with ultrasonication, the flask was placed in 80 °C oil bath, stirred and refluxed to selectively remove Al_2O_3. At certain etching time, some samples were withdrawn, washed repeatedly with water to neutral and dried at 75 °C. The eHA was marked as HA/HCl-*T*, wherein HA, HCl and *T*, respectively, represented halloysite nanotube, HCl as etching solution and etching time.

2.3 The preparation of mesoporous etched halloysite nanotubes supported Co^{2+}

In the preparation of mesoporous eHA supported Co^{2+} (eHA@Co^{2+}), the above eHA without any modification was directly used as the support of Co^{2+} and the concentration of eHA was fixed. A typical process was as follows: eHA (0.50 g), $Co(NO_3)_2 \cdot 6H_2O$ (0.25–2.00 g) and ethanol (100 mL) were added into a 150 mL conical flask. After dispersion with ultrasonication, the flask was stirred at room temperature for 24 h. Then it was separated by centrifugation, washed with ethanol to colourless and dried at 75 °C. This eHA supported Co^{2+} was marked as HA/HCl-*T*/Co^{2+}-*R*, wherein *R* represented the weight ratio of $Co(NO_3)_2 \cdot 6H_2O$ to eHA. Noting: the preparation process can be amplified; when compared with the amount of ethanol (100 mL), the amounts of eHA and $Co(NO_3)_2 \cdot 6H_2O$ were low for well dispersion of eHA and $Co(NO_3)_2 \cdot 6H_2O$ to achieve well dispersion of Co^{2+} in eHA; and the amount of $Co(NO_3)_2 \cdot 6H_2O$ was overdose in order to achieve adsorption saturation.

2.4 Characterization

The morphology of HA/HCl-*T* and HA/HCl-*T*/Co^{2+}-*R* was characterized by JSM-2100 under an accelerating voltage of 200 kV. FT-IR was conducted on a Thermo Nicolet iS10 instrument with KBr pellet as background. The diffuse reflectance spectra of UV-vis were performed on a Hitachi U-4100 PC photometer from 200 to 800 nm. Energy-dispersive X-ray (EDX) analysis was performed with a FEI Quanta-200 scanning electron microscope (SEM) equipped with an EDX analyzer operated at an accelerating voltage of 10 kV. The quantification of the EDX analysis is based on the eZAF Smart Quant method calibrated with pure reference materials-Cu and Al sheet. Nitrogen adsorption–desorption was performed on a Micromeritics (USA) Tristar II 3020. The oxidation product was detected by a gas chromatograph (Agilent 7890A). The gas chromatography was performed in a Agilent 19091J-413 column with a cross-linked 5% phenyl methyl siloxan (30 m × 320 μm × 0.33 mm) and a FID detector under the following conditions:[27] carrier gas (N_2, 40 mL min^{-1}); temperature program-40 °C holding for 2 min, then heating to 50 °C at 10 °C min^{-1}, finally further heating to 300 °C at 50 °C min^{-1}.

2.5 Selective oxidation of cyclohexene by mesoporous etched halloysite nanotubes supported Co^{2+}

Catalyst (HA/HCl-*T*/Co^{2+}-*R*, 40 mg) and cyclohexene (0.8 mL) were added to a 50 mL round-bottom flask. After bubbled with

O_2 for 10 min at appropriate flow rate to avoid the blown away of cyclohexene, the flask was placed in 75 °C oil bath, stirred and refluxed (noting: the joint of the snake-shaped condenser and round-bottom flask must be carefully sealed by PTFE tape, parafilm "M," and electric insulation tape consecutively to avoid the evaporation of cyclohexene). After 18 h, it was separated by centrifugation, then 25 μl supernatant was withdraw and diluted with 1 mL $CHCl_3$ for gas chromatograph characterization.

3 Results and discussion

3.1 Characterization of mesoporous etched halloysite nanotubes supported Co^{2+}

The halloysite nanotube used for synthesis of mesoporous support for Co^{2+} is about 1–2 μm length, 20–30 nm inside diameter and 40–60 nm outside diameter (Fig. S1 in ESI†). It consist of 17.5% Si, 17.6% Al and 64.9% O and with 31.7 $m^2\ g^{-1}$ BET surface area.[19,20,22–27] To demonstrate the Al_2O_3 in halloysite nanotubes can be controlled etched by HCl, the TEM of etched halloysite nanotubes (eHA) at different etching time is given in Fig. 1. It shows when the etching time is 6 h, the inside diameter of eHA increase from the original 20–30 nm to 45–55 nm and the interior surface is coarse. Furthermore, part of the tubular structure has been collapsed (Fig. 1a). This sample is labelled as HA/HCl-6 h. With increase the etching time, for example 7.5 h (HA/HCl-7.5 h) and 11 h (HA/HCl-11 h), nearly all of the interior surface is left exposed accompanied by the disappearance of the inner cavity (Fig. 1b and c). When the etching time is 18 h, porous nanorods with totally lost of the tubular structure are achieved (HA/HCl-18 h) (Fig. 1d). Based on the TEM results, the process for selective etching of Al_2O_3 from HA can be explained as follows: firstly, nanotubes with varying enlargement of the cavity are achieved when a handful of Al_2O_3 is removed; secondly, pores in the HA walls begin to appear and grow with the etching time when more Al_2O_3 is removed; finally, tubular morphology is lost and cavity disappears when the Al_2O_3 is completely removed.[24,28]

FT-IR is further used to characterize the eHA. Along increasing the etching time, the bands intensity of the Al_2OH-stretching (3696 and 3620 cm^{-1}) and the single Al_2OH-bending (912 cm^{-1}) gradually decrease (Fig. 2).[16,24,28] In addition, the bands intensity of Si–O–Al in plane bending mode (754, 692 and 534 cm^{-1}) also show the same trend with the increase of etching time (along further etching). Correspondingly, SiO–H vibrations band at 3200–3700 cm^{-1} appears (the formation of silica) and the band intensity of symmetric Si–O–Si stretching (798 cm^{-1}) increases with the etching time. The above result demonstrates the removal of Al_2O_3 can be controlled.[24,28,29] Eventually, all the Al_2O_3 characteristic bands disappear (trace e, Fig. 2). The Si–O stretching band of halloysite nanotubes (1032 cm^{-1}) completely disappears accompanied by the enhance of the in-plane Si–O–Si deformation peak (1092 cm^{-1}) and the final spectra bear a resemblance to that of amorphous SiO_2.[30] The eHA is further characterized by XRD and EDX. It demonstrates the single 1 : 1 layer aluminosilicate thickness (7.30 Å), other typical reflections of halloysite (4.41 Å, 3.61 Å, 2.49 Å, 2.36 Å, 2.22 Å, 1.68 Å, 1.48 Å) (Fig. S2 in ESI†) and Al/Si atom ratio (Table S1 in ESI†) decrease with etching time, and eventually disappear with a broad band peak present which is attributed to amorphous SiO_2 for XRD and to nearly zero for Al/Si atom ratio, respectively. The above results are consistent with the result of HCl selective etching of octadecyltrichlorosilane silane (C18) modified halloysite nanotube.[24]

The mesoporous structure of eHA is characterized by nitrogen adsorption–desorption. It exhibits clearly halloysite nanotube itself is a mesoporous material (Fig. 3). In addition, according to the International Union of Pure and Applied Chemistry (IUPAC) classification (Fig. 3, Table S2 in ESI†), the adsorption–desorption isotherm of halloysite nanotubes is ascribed to type IV with H3 hysteresis loops as majority of the pore diameter were in the range of 2–8 nm and 15–35 nm.[31] The average pore diameter, pore volume and BET surface area of

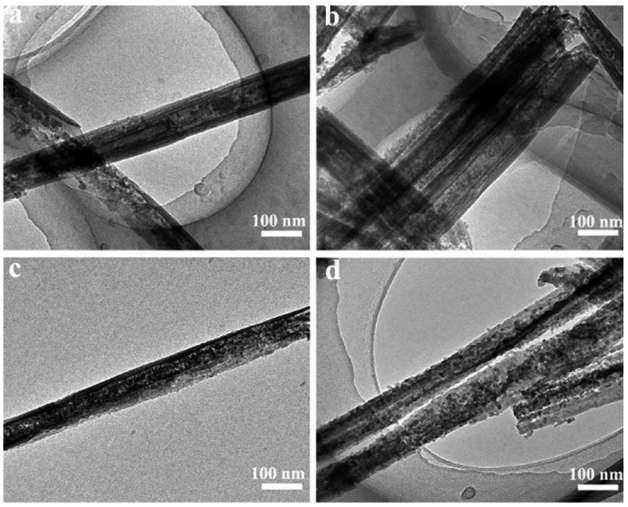

Fig. 1 TEM images of halloysite nanotubes after being etched by HCl at 80 °C for (a) 6 h, (b) 7.5 h, (c) 11 h and (d) 18 h, respectively.

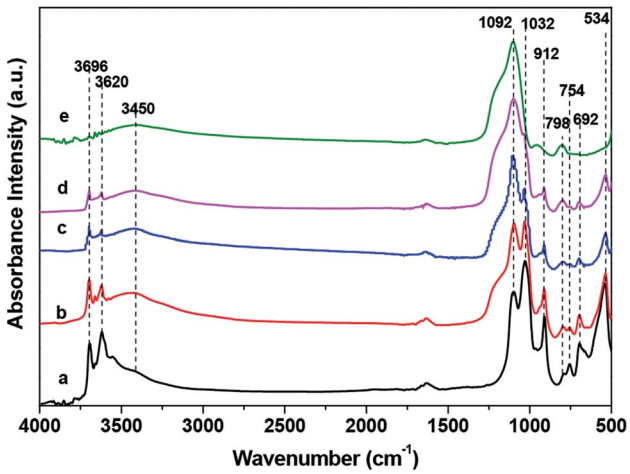

Fig. 2 FT-IR of halloysite nanotubes (a) and halloysite nanotubes after being etched by HCl at 80 °C for (b) 6 h, (c) 7.5 h, (d) 11 h and (e) 18 h, respectively.

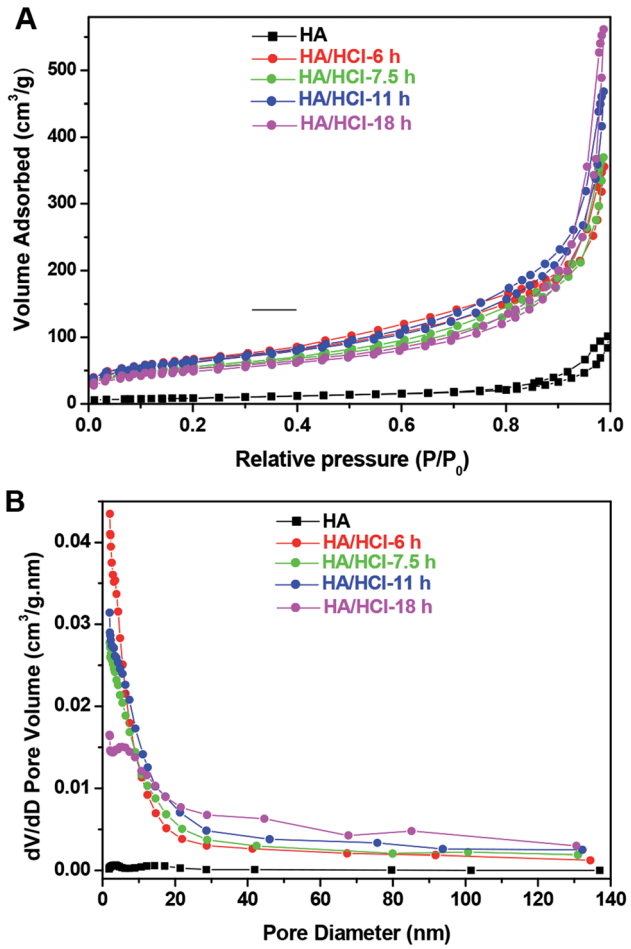

Fig. 3 Nitrogen adsorption–desorption isotherms (A) and pore size distribution curves (B) of halloysite (HA) and HA/HCl-*T*.

halloysite nanotubes are respectively 11.5 nm, 0.16 $cm^3\ g^{-1}$ and 31.7 $cm^2\ g^{-1}$. Compared with those of halloysite nanotubes, the pore volume of eHA is higher and the pore diameter is lower (Fig. 3B, Table S2 in ESI†) when the etching time is lower than 18 h and an opposite situation is observed when the etching time is 18 h (Fig. 3B, Table S2 in ESI†). After selective etching, mesopores in the sizes of 3.0 nm observed in the parent halloysite nanotubes has shifted to larger size, especially for the HA/HCl-18 h sample (has shifted to 5.4 nm), while the pores about 14 nm has shifted to higher position or has disappeared. This indicates that the cavity in the eHA has been partly destroyed or completely disappeared, which is in good agreement with the results of the TEM images. What is deserved to mention that the BET surface area is increased evidently from 31.7 $m^2\ g^{-1}$ for the halloysite nanotube to 176.5 $m^2\ g^{-1}$ for the HA/HCl-6 h sample. However, with further increasing the etching time, the increase of BET surface area is not significant, for example, with the etching time increase from 6 h to 18 h, the BET surface area just increases to 228.4 $m^2\ g^{-1}$ from 176.5 $m^2\ g^{-1}$ (Table S2 in ESI†). The raise of the BET surface area of eHA could be resulted from the selective etching of Al_2O_3 from halloysite nanotubes, which will increase surface roughness and porosity (Fig. 3). It also can be seen with the increase of etching time, the average pore diameter and pore volume of the eHA also increase, implying they can be conditioned by the etching time. As an example, with the increase of etching time from 6 h to 18 h, the average pore diameter and pore volume, respectively, increase from 6.8 nm to 12.0 nm and 0.56 $cm^3\ g^{-1}$ to 0.87 $cm^3\ g^{-1}$.

The above mesoporous eHA is used to support Co^{2+} by an impregnation method and marked as HA/HCl-*T*/Co^{2+}-*R*, wherein *R* represent the weight ratio of $Co(NO_3)_2\cdot 6H_2O$ to eHA. Fig. 4 shows the TEM of HA/HCl-18 h after immerging in different concentration of $Co(NO_3)_2\cdot 6H_2O$ solution. It is demonstrable that the rough/porous structure of HA/HCl-18 h is not affected. Moreover, there are 2.5 nm black spots on eHA and the amount increases with the increase of weight ratio of $Co(NO_3)_2\cdot 6H_2O$ to HA/HCl-18 h (Fig. 4, Table S3 in ESI†). We ascribe them to the Co^{2+} ionic clusters. The Co content of the HA/HCl-18 h/Co^{2+}-*R* is roughly determined by EDX. The FT-IR of eHA@Co^{2+} has no significant difference from that of eHA (Fig. S3 in ESI†). The above results indicate Co^{2+} can be supported on the eHA by the impregnation method and the supported amount of Co^{2+} can be tuned by the feeding amount of weight ratio of $Co(NO_3)_2\cdot 6H_2O$ to HA/HCl-18 h in the preparation. It's hard to ignore that the Al/Si atom ratio and Co content (wt%) determined by EDX are not accurate as there are many factors affecting the EDX test result, for example the flatness/concentrations of sample, the distribution of elements, accelerating voltage of SEM and so on. However, EDX can be used to present the change trend of the Al/Si atom ratio and Co content with the increase of etching time and the weight ratio of $Co(NO_3)_2\cdot 6H_2O$ to eHA, respectively.

3.2 Solvent-free oxidation of cyclohexene to allylic products with oxygen by mesoporous eHA@Co^{2+}

Mesoporous eHA@Co^{2+} (HA/HCl-*T*/Co^{2+}-*R*) is directly used as catalyst for cyclohexene oxidation at 75 °C with O_2 as oxidant

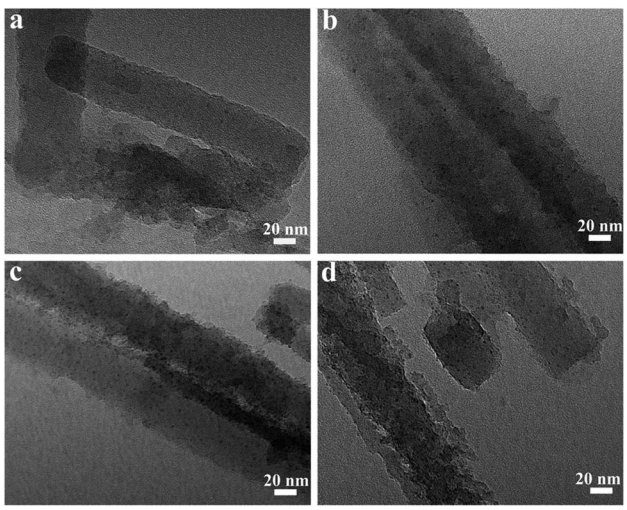

Fig. 4 TEM images of eHA@Co^{2+}: (a) HA/HCl-18 h/Co^{2+}-0.5 : 1, (b) HA/HCl-18 h/Co^{2+}-1 : 1, (c) HA/HCl-18 h/Co^{2+}-2 : 1 and (d) HA/HCl-18 h/Co^{2+}-4 : 1.

(noting: the reaction system is only bubbled with O_2 for 10 min before reaction; during the reaction, no O_2 is bubbled or O_2 balloon is added). And for facilitating comparison, the cyclohexene oxidation efficiency of HA, HA/HCl-18 h (etched with HCl for 18 h, but without supporting Co^{2+}), HA/Co^{2+}-2 : 1 (HA directly supporting Co^{2+} at 2 : 1 weight ratio of $Co(NO_3)_2\cdot 6H_2O$ to HA) and bulk $Co(NO_3)_2\cdot 6H_2O$ are also studied. It is demonstrable that cyclohexene oxidation with HA, HA/HCl-18 h and HA/Co^{2+}-2 : 1 as catalyst and catalyst-free demonstrates extremely low cyclohexene conversion (1.63%, 9.30%, 9.58% and 8.13%, respectively). Nevertheless with HA/HCl-*T*/Co^{2+}-*R* as catalyst, cyclohexene conversion increase significantly, for example, with HA/HCl-18 h/Co^{2+}-2 : 1 as catalyst, the cyclohexene conversion increases to 58.30%. In combination of 9.58% and 9.30% cyclohexene conversion with HA/Co^{2+}-2 : 1 and HA/HCl-18 h as catalyst, respectively, the above results signify both of the porous structure of eHA and supported Co^{2+} are contributed to the enhanced cyclohexene oxidation activity of HA/HCl-*T*/Co^{2+}-*R*. However, the cyclohexene oxidation efficiency of HA/HCl-*T*/Co^{2+}-*R* is varied along the change of etching time (*T*) and weight ratio of $Co(NO_3)_2\cdot 6H_2O$ to eHA (*R*) in the preparation. For the influence of etching time, at 2 : 1 weight ratio of $Co(NO_3)_2\cdot 6H_2O$ to eHA, cyclohexene conversion increase with the etching time. For example, when the etching time increases from 0 h to 18 h, the cyclohexene conversion increases from 9.58% to 58.30% and an optimal etching time is 18 h (Entry 2–6, Table 1). The tendency is consistent with the BET surface area of eHA (longer etching time will result in higher BET surface area, which finally lead to higher Co^{2+} supporting content). Evidently, the etching time in the preparation will affect the cyclohexene oxidation efficiency of HA/HCl-*T*/Co^{2+}-*R*.

For the effect of weight ratio of $Co(NO_3)_2\cdot 6H_2O$ to eHA in the preparation, when the weight ratio of $Co(NO_3)_2\cdot 6H_2O$ to eHA is between 0.5 : 1–2 : 1 (Table 1, Fig. S4 in ESI†), cyclohexene conversion increases with the increase of $Co(NO_3)_2\cdot 6H_2O$/eHA weight ratio, and then when the $Co(NO_3)_2\cdot 6H_2O$/eHA weight ratio is in the range of 2 : 1–4 : 1, the cyclohexene conversion decreases with the increase of $Co(NO_3)_2\cdot 6H_2O$/eHA weight ratio. An optimal $Co(NO_3)_2\cdot 6H_2O$/eHA weight ratio in the fabrication is 2 : 1. The effect of $Co(NO_3)_2\cdot 6H_2O$/eHA weight ratio on the conversion is attributed to a cooperative effect of Co content and Co^{2+} dispersion on the eHA. Combined with the EDX result that the Co content increases with the increase of $Co(NO_3)_2\cdot 6H_2O$/eHA weight ratio (Table S3 in ESI†), the cyclohexene oxidation efficiency of HA/HCl-*T*/Co^{2+}-*R* will be affected by the Co content in the mesoporous eHA@Co^{2+} ($Co(NO_3)_2\cdot 6H_2O$/eHA weight ratio in the preparation). It is deserved to mention that the cyclohexene conversion, TON and r_w of HA/HCl-18 h/Co^{2+}-2 : 1 are higher than those of the bulk $Co(NO_3)_2\cdot 6H_2O$ (Entry 6, 14, Table 1) at the equivalent amount of Co, indicating the porous structure of HA/HCl-18 h can well disperse Co^{2+}. About the selectivity, the main oxidation products are allylic products (2-cyclohexen-1-one and 2-cyclohexen-1-ol) and the selectivity to allylic products accounts for more than 90%.

Furthermore, as the chemical composition of HA is $Al_2Si_2O_5(OH)_4\cdot nH_2O$), the SiO_2 in HA can be selectively etched by NaOH. The sample etched by NaOH for 18 h (HA/NaOH-18 h) is used to support Co^{2+} with 1 : 1, 2 : 1 and 4 : 1 weight ratio of $Co(NO_3)_2\cdot 6H_2O$ to HA/NaOH-18 h. It still shows the optimal weight ratio is 2 : 1, which achieves 29.06% cyclohexene conversion. For the oxidation product of HA/NaOH-18 h/Co^{2+}-*R*, it is still allylic product (the selectivity is higher than 79%). However, the catalytic activity of HA/NaOH-18 h/Co^{2+}-*R* is lower than that of HA/HCl-18 h/Co^{2+}-*R* at the same weight ratio of $Co(NO_3)_2\cdot 6H_2O$ to eHA, indicating HA/HCl-*T* can support more Co^{2+} owing to the negative charged of SiO_2 in HA/HCl-*T*.

Notably, the selectivity to allylic product of cyclohexene oxidation catalyzed by HA/HCl-*T*/Co^{2+}-*R* exceeds 90%, independence on the etching time and $Co(NO_3)_2\cdot 6H_2O$/eHA weight ratio in the preparation, which will simplify the later purification and separation. The cyclohexene conversion and selectivity to allylic products (2-cyclohexen-1-one and 2-cyclohexen-1-ol) with HA/HCl-18 h/Co^{2+}-2 : 1 as catalyst are 58.30% and 94.03% respectively, indicating it can selectively oxidize cyclohexene to allylic products. Both of the cyclohexene conversion and selectivity to allylic products are higher than that of Co(II)-containing MOFs (Co-MOF, 32.80% conversion and 90.80% selectivity to allylic products), even both the reaction temperature (75 °C) and time (18 h) are lower than that of Co(II)-containing MOFs (80 °C and 20 h) and the simplification of oxidation process (only bubbled with O_2 for 10 min before reaction; during the reaction, no O_2 is bubbled or O_2 balloon is added).[6] Based on the above results, the etching time and $Co(NO_3)_2\cdot 6H_2O$/eHA weight ratio in the preparation will exert a significant impact on the cyclohexene oxidation efficiency of HA/HCl-*T*/Co^{2+}-*R*. Thereinto, HA/HCl-18 h/Co^{2+}-2 : 1 performs the highest catalytic efficiency, corresponding to a 1209.98 TON and 1140.69 mmol g^{-1} h^{-1} mass-normalized activity. This activity is significantly higher than that of halloysite nanotubes supported PANI (PANI@HA/1 M/2.04-HCl, 148.66 TON and 67.33 mmol g^{-1} h^{-1})[27] and Co(II)-containing metal–organic frameworks (MOFs) (Co-MOF, 80.22 TON and 68.07 mmol g^{-1} h^{-1}).[6] So HA/HCl-18 h/Co^{2+}-2 : 1 is an effective catalyst for allylic oxidation of cyclohexene and chosen for further studies.

Furthermore, the effect of calcinations on the cyclohexene catalytic oxidation activity of HA/HCl-18 h/Co^{2+}-2 : 1 and HA/NaOH-18 h/Co^{2+}-2 : 1 is investigated. HA/HCl-18 h/Co^{2+}-2 : 1 and HA/NaOH-18 h/Co^{2+}-2 : 1 are treated at 550 °C for 6 h, cited as HA/HCl-18 h/Co^{2+}-2 : 1/550 °C-6 h and HA/NaOH-18 h/Co^{2+}-2 : 1/550 °C-6 h, respectively (Entry 2 and 4, Table S4 in ESI†). And they are used as catalyst and compared with those without calcinations (Entry 1 and 3, Table S4 in ESI†). It is demonstrable calcinations will decrease the catalytic activity of HA/HCl-18 h/Co^{2+}-2 : 1, whereas it has a positive effect on HA/NaOH-18 h/Co^{2+}-2 : 1. It can be explained by the fact calcinations will lead to the aggregation of Co^{2+} or cobalt oxide for HA/HCl-18 h/Co^{2+}-2 : 1 owing to the adsorption saturation of Co^{2+} on HA/HCl-18 h/Co^{2+}-2 : 1, whereas it will solid the adsorbed Co^{2+} on HA/NaOH-18 h/Co^{2+}-2 : 1 because NaOH etching will lead to partly positive charged Al_2O_3, which will produce electrostatic repulsion to Co^{2+}. Therefore, HA/HCl-18 h/Co^{2+}-2 : 1 is selected for optimization of reaction condition.

Table 1 Cyclohexene conversion and selectivity of HA/HCl-*T*/Co^{2+}-*R* and HA/NaOH-*T*/Co^{2+}-*R*

Catalyst	Selectivity (%) 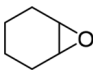	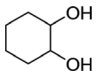			Conversion (%)	TON[a]	r_w[b](mmol g^{-1} h)
HA	0	5.52	59.74	34.74	1.63	—	—
HA/Co^{2+}-2 : 1	0	10.76	45.86	43.38	9.58	—	—
HA/HCl-6 h/Co^{2+}-2 : 1	0	5.10	69.02	25.88	10.49	—	—
HA/HCl-7.5 h/Co^{2+}-2 : 1	0	8.97	53.36	37.66	16.82	—	—
HA/HCl-11 h/Co^{2+}-2 : 1	0.45	5.14	65.57	28.84	23.92	—	—
HA/HCl-18 h/Co^{2+}-2 : 1	0.27	5.70	54.60	39.43	58.30	1209.98	1140.69
HA/HCl-18 h	1.51	0	59.17	39.31	9.30	—	—
HA/HCl-18 h/Co^{2+}-0.5 : 1	3.34	1.10	51.73	43.83	18.33	1065.20	1004.20
HA/HCl-18 h/Co^{2+}-1 : 1	3.50	4.88	49.16	42.46	26.63	644.80	607.88
HA/HCl-18 h/Co^{2+}-4 : 1	1.09	4.70	60.68	33.53	29.27	507.74	478.67
HA/NaOH-18 h/Co^{2+}-1 : 1	1.10	8.76	49.22	40.93	19.21	—	—
HA/NaOH-18 h/Co^{2+}-2 : 1	2.05	17.95	54.22	25.77	29.06	—	—
HA/NaOH-18 h/Co^{2+}-4 : 1	0.82	7.48	60.02	31.68	22.51	—	—
$Co(NO_3)_2 \cdot 6H_2O$[c]	5.40	3.52	60.87	30.20	13.59	282.05	265.90
Catalyst-free	5.20	50.34	14.68	29.78	8.13	—	—
Halloysite nanotubes supported PANI (PANI@HA/1 M/2.04-HCl)[d]	0	99.50	0.05	0.45	98.17	148.66	67.33
Co(II)-containing metal–organic frameworks[e]	3.05	0	51.26	39.34	32.80	80.22	68.07

Reaction conditions: 40 mg catalyst, 0.8 mL cyclohexene, O_2 (10 min), 75 °C, 18 h. [a] TON (turnover number) is defined as total mol of cyclohexene molecules converted per mol of catalyst. [b] Initial reaction rate of cyclohexene consumption normalized by catalyst mass. [c] The added amount of $Co(NO_3)_2 \cdot 6H_2O$ is 1.1 mg, comparable to the amount of Co in 40 mg HA/HCl-18 h/Co^{2+}-2 : 1. [d] Reaction conditions: 20 mg catalyst, 1.23 mL cyclohexene, 2.5 mL H_2O_2, 70 °C, 24 h (ref. 27). [e] Reaction conditions: 50 mg catalyst, 5 mL cyclohexene, oxygen balloon, 80 °C, 20 h (ref. 6).

In the next, optimization of reaction condition (such as oxidant, solvent, reaction time and reaction temperature) for cyclohexene oxidation by HA/HCl-18 h/Co^{2+}-2 : 1 is further undergoing. At first, the effect of oxidant on cyclohexene oxidation is investigated. Considering environmentally-friendly aspect, O_2 and 30% H_2O_2 are chosen as oxidant. The detailed result is shown on Table S5.† It is clearly when bubbling O_2 for 10 min before oxidation, cyclohexene conversion achieves 58.30%; whereas without bubbling O_2, the conversion is only 10.41%. Combined with 10.41% cyclohexene conversion of HA/HCl-18 h/Co^{2+}-2 : 1 without bubbling O_2 (Entry 2, Table S5 in ESI†) and 9.30% cyclohexene conversion with HA/HCl-18 h as catalyst and O_2 as oxidant (Entry 7, Table 1), we conclude that the role of Co in HA/HCl-18 h/Co^{2+}-2 : 1 should be catalysized O_2 to achieve active oxygen species. Whereas, with H_2O_2 as oxidant, the cyclohexene conversion is very low, only 25.70% and the main oxidation product is 1,2-cyclohexandiol (98.70% selectivity), demonstrating under O_2 and 30% H_2O_2, cyclohexene oxidation catalyzed by HA/HCl-18 h/Co^{2+}-2 : 1 undergoes different pathway. Considering the facilitation of later purification and allylic products as the main oxidation with O_2 as oxidant, O_2 is selected as oxidant in the current catalytic reaction system.[27]

In the following, the effect of solvent (CH_3CN, CH_2Cl_2, THF, DMF, *n*-heptane and acetic anhydride) on the selective oxidation of cyclohexene is investigated and compared with the solvent-free reaction system. Noting: the volume of solvent is six times (4.8 mL) the volume of cyclohexene (0.8 mL) to avoid the evaporation of cyclohexene in the oxidation process. The result is in Table S6.† It is obvious the catalytic efficiency of the solvent-free reaction system is higher when compared with the solvent reaction system (58.30% cyclohexene conversion and 94.03% allylic products selectivity). It can also be observed that high polar solvents (acetic anhydride and DMF) can result in the selectivity to allylic products (57.70% and 76.70% for acetic anhydride and DMF, respectively) decreasing and accompany the selectivity to epoxy cyclohexane (20.00% for DMF) and 1,2-cyclohexanediol (41.80% for acetic anhydride) increasing (Table S6 in ESI†). It could be under the high polar solvent, the epoxy cyclohexene and 1,2-cyclohexanediol can easily desorb from the catalyst, thus facilitating the formation of epoxy cyclohexene and 1,2-cyclohexanediol.[27,32]

Other reaction condition, for example, the effect of reaction temperature (20–80 °C) and reaction time (0–24 h) is further investigated. It shows that the cyclohexene conversion increases significantly with the increase of reaction temperature when the reaction temperature is in the range of 20–75 °C and the conversion achieves 58.30% with 94.03% allylic products selectivity when the reaction temperature is 75 °C (Fig. S5 and Table S7 in ESI†). The increase of catalytic efficiency with the reaction temperature may be ascribed to the fact high temperature can afford sufficient energy for selective oxidation of

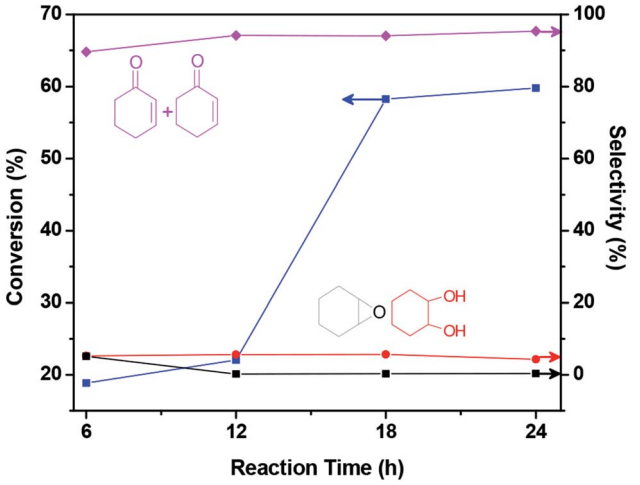

Fig. 5 The effect of reaction time on the cyclohexene conversion and selectivity of HA/HCl-18 h/Co^{2+}-2 : 1.

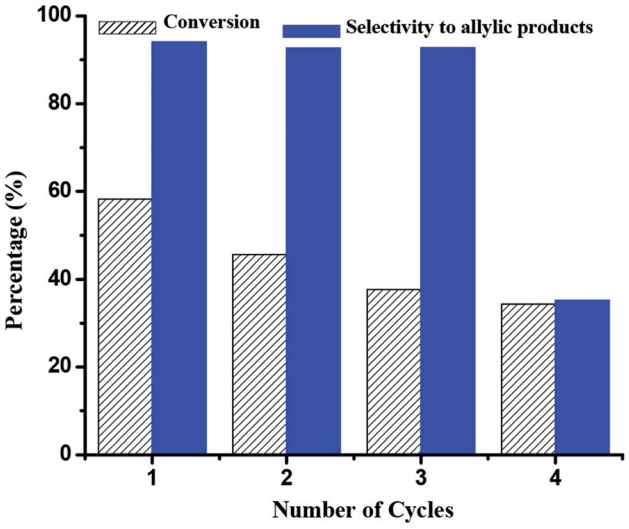

Fig. 6 The cycling stability of cyclohexene oxidation with HA/HCl-18 h/Co^{2+}-2 : 1 as catalyst.

cyclohexene.[27] Then the cyclohexene conversion increases indistinctly when the cyclohexene oxidation is conducted at 80 °C. So 75 °C is selected as reaction temperature in the following studies. It is worth mentioning the selectivity to allylic products stays at a high level (>90%) when the reaction temperature is at 20–80 °C. For the effect of reaction time, when the reaction time is 6 h, the conversion is only 18.84%; nevertheless when the reaction time is 18 h, the conversion quickly increases to 58.30%; with further increasing the reaction time, the conversion increases slightly (Fig. 5, Table S8 in ESI†). And the selectivity to allylic products is higher than 89% within 6–24 h reaction time, indicating during the oxidation process, the main oxidation products are allylic products. So the reaction time is fixed at 18 h for cyclohexene oxidation.

3.3 Cycling stability of mesoporous etched halloysite nanotubes supported Co^{2+}

Stability and recycling is an important index for catalyst.[6–15,27] The cycling stability experiments are conducted with HA/HCl-18 h/Co^{2+}-2 : 1 as catalyst and each cycle of the reaction time is 18 h. After each cycle, HA/HCl-18 h/Co^{2+}-2 : 1 is separated by centrifugation, washed by CH_2Cl_2, dried consecutively and used as catalyst for the next cycle of cyclohexene oxidation. The results are concluded in Fig. 6 and Table S9.† There are strong signs that cyclohexene conversion decreases slightly after four cycles, whereas allylic product selectivity demonstrates different trend, which maintains higher value (>92%) in the first three cycles, but decrease to 35.21% in the fourth cycle. Considering the sharp declination to allylic product selectivity, we attribute it to the dissolution of Co^{2+} in the cycling experiment. However, it still indicates HA/HCl-18 h/Co^{2+}-2 : 1 can be recycled three times effectively for cyclohexene oxidation. Considering the green catalytic reaction system (solvent-free, green oxidant and simple and convenient style of adding O_2), high allylic product selectivity and good cycling stability, it will promote to purification and has potential application prospect in the fine chemical industry.

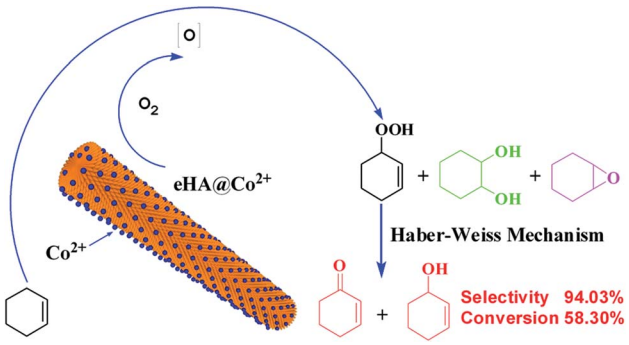

Scheme 1 Proposed mechanism of cyclohexene selective oxidation to allylic product (2-cyclohexen-1-one and 2-cyclohexen-1-ol) with mesoporous eHA@Co^{2+} as catalyst.

3.4 Cyclohexene selective oxidation mechanism of mesoporous etched halloysite nanotubes supported Co^{2+}

Based on the above results, a mechanism for the allylic oxidation of cyclohexene over mesoporous eHA supported Co^{2+} is proposed as follows: firstly, O_2 will bind to the Co^{2+} in mesoporous eHA supported Co^{2+} (eHA@Co^{2+}), leading to the form of O_2-eHA@Co^{2+} adduct; secondly, O_2-eHA@Co^{2+} adduct abstracts H atom from cyclohexene to form cyclohexenyl radicals and hydroperoxo complex (eHA@Co^{3+}–OOH) synchronously. Then peroxy radical (HOO˙) will be produced by cracking the Co^{3+}–OOH bond, accompanied by the recovery of eHA@Co^{2+}. The peroxy radical will react with cyclohexenyl radicals to achieve 2-cyclohexene-1-hydroperoxide (reaction intermediate) (Scheme 1).[6,7] Finally, the formed 2-cyclohexene-1-hydroperoxide will be decomposed into allylic oxidation products (2-cyclohexen-1-one and 2-cyclohexen-1-ol) according to the Haber–Weiss mechanism, which involved in the Co cycling of Co^{3+} and Co^{2+}.[33,34]

4 Conclusions

Mesoporous eHA@Co^{2+} nanotubes or nanorods have been successfully fabricated by in combination of HCl selective etching of interior Al_2O_3 from halloysite nanotubes and the impregnation method. Mesoporous eHA@Co^{2+} endowing different BET surface area and Co^{2+} content can be achieved by simply tuning the etching time and the weight ratio of $Co(NO_3)_2 \cdot 6H_2O$ to eHA in the preparation. The mesoporous eHA@Co^{2+} prepared with 18 h etching time and 2 : 1 $Co(NO_3)_2 \cdot 6H_2O$/eHA weight ratio (HA/HCl-18 h/Co^{2+}-2 : 1) shows the highest BET surface area and high Co^{2+} content. The influence of etching time and $Co(NO_3)_2 \cdot 6H_2O$/eHA weight ratio in the fabrication of eHA@Co^{2+} on the cyclohexene selective oxidation are pored through. It indicates HA/HCl-18 h/Co^{2+}-2 : 1 demonstrates the highest cyclohexene conversion (58.30%) and the dominant oxidation products are 2-cyclohexen-1-one and 2-cyclohexen-1-ol in solvent-free reaction system with one-time bubbled O_2 as oxidants. And cyclohexene catalytic oxidation efficiency hinges on the etching time and the weight ratio of $Co(NO_3)_2 \cdot 6H_2O$ to eHA in the preparation. The optimal reaction condition is 75 °C, 18 h, solvent-free and O_2 as oxidant for cyclohexene oxidation to allylic product. According to the experiment result, a mechanism for cyclohexene oxidation attributed to reversible Co cycling between Co^{3+} and Co^{2+} in eHA@Co^{2+} to catalytic formation of active [O] is suggested. This work not only provides a facilitate method to large scale synthesis of mesoporous support to achieve eHA@Co^{2+} nanorods and nanotubes, which avoids the surfactant, but also affords an efficient catalyst for cyclohexene selective oxidation to allylic product. Owing to the environmentally friendly reaction system (solvent-free and one-time bubbled O_2 as oxidant), this work may highlight the prospect of developing mesoporous support for Co^{2+} as green and recyclable heterogeneous catalysts in allylic oxidation.

Conflicts of interest

There are no conflicts to declare.

Acknowledgements

The authors gratefully acknowledge the financial support provided by the National Natural Science Foundation of China (No. 51563023 and 51003091), the Natural Science Foundation of Yunnan Province (No. 2013FB002), the Education Research Foundation of Yunnan Province (No. 2013Y361), the Program for Excellent Young Talents, Yunnan University (No. WX069051) and the Backbone Teacher Training Program of Yunnan University (No. 21132014).

Notes and references

1 Y. Cao, H. Yu, H. Wang and F. Peng, *Catal. Commun.*, 2017, **88**, 99.
2 T. Imahori, T. Tokuda, T. Taguchi and H. Takahata, *Org. Lett.*, 2012, **14**, 1172.
3 M. Sipiczki, A. A. Ádám, T. Anitics, Z. Csendes, G. Peintler, Á. Kukovecz, Z. Kónya, P. Sipos and I. Pálinkó, *Catal. Today*, 2015, **241**, 231.
4 X. Liu and C. M. Friend, *Langmuir*, 2010, **26**, 16552.
5 G. Yang, M. D. Huff, H. Du, Z. Zhang and Y. Lei, *Catal. Commun.*, 2017, **99**, 43.
6 Y. Fu, D. Sun, M. Qin, R. Huang and Z. Li, *RSC Adv.*, 2012, **2**, 3309.
7 D. Sun, F. Sun, X. Deng and Z. Li, *Inorg. Chem.*, 2015, **54**, 8639.
8 P. Bujak, P. Bartczak and J. Polanski, *J. Catal.*, 2012, **295**, 15.
9 Y. Cao, H. Yu, F. Peng and H. Wang, *ACS Catal.*, 2014, **4**, 1617.
10 Y. Chang, Y. Lv, F. Lu, F. Zha and Z. Lei, *J. Mol. Catal. A: Chem.*, 2010, **320**, 56.
11 A. Abdolmaleki and S. R. Adariani, *Catal. Commun.*, 2015, **59**, 97.
12 N. R. Khalili, R. Rahimi and M. Rabbani, *Monatsh. Chem.*, 2013, **144**, 597.
13 A. K. Rahiman, S. Sreedaran, K. S. Bharathi and V. Narayanan, *J. Porous Mater.*, 2010, **17**, 711.
14 E. Y. Jeong, A. Burri, S. Y. Lee and S. E. Park, *J. Mater. Chem.*, 2010, **20**, 10869.
15 C. M. Chanquia, A. L. Canepa, K. Sapag, P. Reyes, E. R. Herrero, S. G. Casuscelli and G. A. Eimer, *Top. Catal.*, 2011, **54**, 16.
16 E. Joussein, S. Petit, J. Churchman, B. Theng, D. Righi and B. Delvaux, *Clay Miner.*, 2005, **40**, 383.
17 G. J. Churchman and R. M. Carr, *Clays Clay Miner.*, 1975, **23**, 382.
18 S. Barrientos-Ramırez, E. V. Ramos-Fernandez, J. Silvestre-Albero, A. Sepulveda-Escribano, M. M. Pastor-Blas and A. Gonzalez-Montiel, *Microporous Mesoporous Mater.*, 2009, **120**, 132.
19 C. Li, X. Li, X. Duan, G. Li and J. Wang, *J. Colloid Interface Sci.*, 2014, **436**, 70.
20 C. Li, J. Wang, S. Feng, Z. Yang and S. Ding, *J. Mater. Chem. A*, 2013, **1**, 8045.
21 E. Abdullayev, K. Sakakibara, K. Okamoto, W. Wey, K. Ariga and Y. Lvov, *ACS Appl. Mater. Interfaces*, 2011, **3**, 4040.
22 J. Liang, B. Dong, S. Ding, C. Li, B. Q. Li, J. Li and G. Yang, *J. Mater. Chem. A*, 2014, **2**, 11299.
23 C. Li, T. Zhou, T. Zhu and X. Li, *RSC Adv.*, 2015, **5**, 98482.
24 C. Li, J. Wang, X. Luo and S. Ding, *J. Colloid Interface Sci.*, 2014, **420**, 1.
25 C. Li, J. Wang, H. Guo and S. Ding, *J. Colloid Interface Sci.*, 2015, **458**, 1.
26 T. Zhou, C. Li, H. Jin, Y. Lian and W. Han, *ACS Appl. Mater. Interfaces*, 2017, **9**, 6030.
27 T. Zhou, Y. Zhao, W. Han, H. Xie, C. Li and M. Yuan, *J. Mater. Chem. A*, 2017, **5**, 18230.
28 E. Abdullayev, A. Joshi, W. Wei, Y. Zhao and Y. Lvov, *ACS Nano*, 2012, **6**, 7216.
29 H. W. van der Marel and H. Beutelspacher, *Atlas of Infrared Spectroscopy of Clay Minerals and their Admixtures.*, Elsevier scientific publishing company, New York, 1976.

30 Z. Wang, Q. Liu, J. Yu, T. Wu and G. Wang, *Appl. Catal., A*, 2003, **239**, 87.
31 K. S. W. Sing, D. H. Everett, R. A. W. Haul, L. Moscou, R. A. Pierotti, N. Rouquerol and T. Siemieniewska, *Pure Appl. Chem.*, 1985, **57**, 603.
32 J. C. Torres, D. Cardoso and R. Pereira, *Microporous Mesoporous Mater.*, 2010, **136**, 97.
33 D. E. Hamilton, R. S. Drago and A. Zombeck, *J. Am. Chem. Soc.*, 1987, **109**, 374.
34 H. Weiner, A. Trovarelli and R. G. Finke, *J. Mol. Catal. A: Chem.*, 2003, **191**, 217.